AIP | Journal of Applied Physics

Ultrafast ablation with high-pulse-rate lasers. Part II: Experiments on laser deposition of amorphous carbon films

A. V. Rode, B. Luther-Davies, and E. G. Gamaly

Citation: Journal of Applied Physics **85**, 4222 (1999); doi: 10.1063/1.370334
View online: http://dx.doi.org/10.1063/1.370334
View Table of Contents: http://scitation.aip.org/content/aip/journal/jap/85/8?ver=pdfcov
Published by the AIP Publishing

JOURNAL OF APPLIED PHYSICS VOLUME 85, NUMBER 8 15 APRIL 1999

Ultrafast ablation with high-pulse-rate lasers. Part II: Experiments on laser deposition of amorphous carbon films

A. V. Rode[a] and B. Luther-Davies
Laser Physics Centre, Research School of Physical Science and Engineering, Australian National University, Canberra, ACT 0200, Australia

E. G. Gamaly
Universidad Autonoma Metropolitana, Departamento de Fisica, Apartado Postal 55-534, Iztapalapa, C.P. 09340 Mexico, D.F

(Received 4 June 1998; accepted for publication 14 December 1998)

Ultrafast pulsed laser deposition is a novel technique for depositing particle-free, thin solid films using very high repetition rate lasers. The process involves evaporation of the target by low energy laser pulses focused to an optimum intensity to eliminate particles from the vapor. This results in films with very high surface quality while the very high repetition rate increases the overall deposition rate. Here we report an experimental demonstration of the process by creating ultrasmooth, thin, amorphous carbon films using high repetition rate Nd:YAG lasers. Both a 10 kHz, 120 ns *Q*-switched Nd:YAG laser, or a 76 MHz 60 ps mode-locked Nd:YAG laser were used in the experiments. The number of particles visible with an optical microscope on the carbon film deposited using the mode-locked laser was less than one particle per mm^2. Scanning electron microscopy images demonstrated that the deposited film had a very fine surface texture with nanoscale irregularities. Atomic force microscopy surface microroughness measurements revealed a saturation-like behavior of the root-mean-square roughness at <12 nm over the whole deposited surface area for 10 kHz *Q*-switched laser evaporation; and almost at the atomic level (<1 nm) for the 76 MHz mode-locked laser evaporation. Raman spectroscopy of the deposited films indicated that they consisted of a mixture of sp^3 and sp^2 bonded amorphous carbon. The thickness of the amorphous carbon film deposited simultaneously on two 4 in. silicon wafers varied by only $\pm 5\%$ over an area of ~ 250 cm^2. The deposition rate was ~ 2–6 Å/s at a distance of ~ 150 mm from the target, which is 10 to 25 times higher than that achieved with conventional high energy low repetition rate nanosecond lasers. © *1999 American Institute of Physics.*
[S0021-8979(99)07407-1]

I. INTRODUCTION

During the past decade, pulsed laser deposition (PLD) has been successfully applied to the preparation of thin films of many different materials.[1] Lasers of various wavelength (from 193 nm to 10.6 μm); pulse duration (from tens of femtoseconds to hundreds of nanoseconds); and intensity have been used in these studies. However, the use of energetic lasers producing ≈ 10 ns duration pulses at 10–50 Hz repetition rate has become standard practice in PLD. At these repetition rates, the vapor plume decays away between pulses and, therefore, the film grows in a discontinuous manner from bursts of atoms arriving separately at the substrate. Continuous growth of a film can, however, occur if a continuous flow of atomic vapors with regulated atomic velocity (temperature) and flux can be generated. In fact, as the laser repetition rate used in PLD increases, it is possible to reach this condition because the spread of atom velocities in the laser evaporated plume means that the slow atoms from one pulse arrive at the same time as the faster atoms from following pulses. The method for generating this kind of flow of atomic vapor has been proposed and theoretically justified in the accompanying article[2] (referred to here as part I) and this lays the theoretical basis for the experimental studies reported here.

It was postulated in Ref. 2, that a change from the conventional high energy, low repetition rate lasers used for PLD, to lasers with low pulse energy and repetition rates in ≈ 10 kHz to >10 MHz range, would lead to a significant improvement in the quality of the deposited films due to the reduction, by several orders of magnitude, in the number of atoms evaporated by each laser pulse. In particular, the problem of ejection of clumps of solid material from the target, which occurs when high-energy pulses are used, can be totally eliminated. A proper combination of laser pulse intensity and duration is needed to optimize ablation in this so-called ultrafast PLD regime, and this is determined by the thermodynamic parameters of the target (its specific heat, vaporization temperature, and thermal conductivity). Ultrafast PLD can obviously be extended to the formation of structured and multilayered films of different materials.

This article (part II) presents experimental results on evaporation of carbon by two high repetition rate Nd:YAG lasers: one is a 10 kHz *Q*-switched ''LEE'' laser; and the other is a 76 MHz, mode-locked ''Antares'' laser. Some of the results, such as particle density on the film surface, were

[a]Electronic mail: avr111@rsphy1.anu.edu.au

compared to those obtained from PLD using a 20 ns, 30 Hz, high energy, Q-switched Nd laser.

Graphite was chosen as the target material for testing ultrafast PLD for the following reasons. First, carbon is one of the most refractory materials in nature, therefore, the demonstration of effective carbon evaporation would serve as a proof of the possibility of evaporating almost all other materials which absorb laser radiation. Second, as a first demonstration of ultrafast PLD we have prepared high surface quality amorphous carbon (a-C) films which have potential for a wide range of industrial and scientific applications.

The article is structured as follows. In Sec. II we describe the experimental apparatus and the diagnostics methods used. Section III presents the experimental results on the diagnostics of the laser plume and the characterization of the deposited carbon film. Optical emission spectra from the vapors in the laser plume allowed its ion composition to be defined and provided a comparison of different laser–target interaction modes. The images of the laser plume demonstrate a drastic reduction in the ejection of particulates from the target. Measurements of the target evaporation rate using single and multiple pulse modes illustrate the importance of scanning the laser beam over the target surface during high repetition rate laser evaporation. Studies of the optical characteristics of the deposited carbon films were performed by optical ellipsometry and Raman spectroscopy, while the film surface quality was tested by using optical microscopy, scanning electron microscopy, and atomic force microscopy. We discuss the results and compare them to the theoretical predictions and with previous studies while our conclusions are presented in Sec. IV.

II. EXPERIMENTAL SETUP AND DIAGNOSTICS

A. Laser radiation

The experimental apparatus for ultrafast PLD used two high average power, high repetition rate, Nd:YAG lasers ($\lambda = 1.064\,\mu$m): one being a 42 W, 2–25 kHz, 120 ns Q-switched multimode laser (produced by Lee Laser Corporation, model 708TQG) with laser energy per pulse ~3 mJ at 10 kHz (25 kW peak power); and the other was a 23 W, 76 MHz, 60 ps mode-locked single mode Antares laser (produced by Coherent Laser Corporation, model 76-S), with laser energy per pulse ~300 nJ (5 kW peak power).

The laser radiation was focused on the target surface using a lens optimized for laser scanning (Special Optics, model 55-S236-150) which allowed the bean to be scanned over an area of the target surface up to ~230 cm^2 without altering the focal spot diameter. The absorbed laser intensity at the target was measured using two high-speed photodetectors, both covered with interference filters for 1064 μm: one measured the incoming laser energy, and the other the laser energy back reflected into the aperture of the focusing lens. The reflected signal was 6%–8% of the incoming laser radiation. This measurement provided strong evidence that the laser radiation was effectively absorbed (85%–90%) either in the graphite target and in the carbon vapor near the target surface.

According to the theoretical predictions,[2] the required laser intensity on the target surface for optimal evaporation of the target depends on the laser pulse duration. The relationship for the optimal absorbed laser intensity I_a and pulse duration t_p for a graphite target is[2]

$$I_a\sqrt{t_p} = 1.89\times 10^5\left[\frac{J}{\mathrm{cm^2\,s^{1/2}}}\right]. \tag{1}$$

Thus, for $t_p \approx 120$ ns, $I_a = 6\times 10^8$ W/cm^2 which corresponds to a laser fluence of ~70 J/cm^2. This indicates that the average power required from the Q-switched laser is ~25–30 W for a focal spot ~60–70 μm in diameter, and a laser repetition rate of ≈10 kHz.

Precise measurements of the pulse duration of the mode-locked laser, performed using a standard second harmonic autocorrelator, yielded a value of 60 ± 5 ps full-width at half-maximum (FWHM). The optimal absorbed laser intensity for a 60 ps pulse is 2.4×10^{10} W/cm^2 (which corresponds to a laser fluence of 1.44 J/cm^2. In order to approach such a high intensity, the TEM_{00} beam from the Antares laser was expanded by a Galilean telescope to 25 mm diameter and focused to a spot of 15 μm in diameter. The resulting peak laser intensity 2.8×10^9 W/cm^2 on the target surface is almost an order of magnitude lower than the required for the optimal regime. Nevertheless, it proved effective for evaporation of the graphite target. Despite the fact that the intensity of the mode-locked laser was not optimal, it was still possible to demonstrate some advantages of ultrafast laser evaporation (high evaporation speed; wide angular distribution; very high quality film surface) by comparing the results of 10 kHz laser evaporation with that from the 76 MHz laser.

B. Vacuum chamber

PLD was performed in a chamber evacuated using a diffusion pump to 10^{-6} Torr. The laser beam was focused on a graphite cylinder 50 mm in diameter normal to its cylindrical surface. The cylinder could be rotated around its axis with variable speed up to 1500 rev/min. The speed of rotation was adjusted depending on the laser repetition rate. For 10 kHz repetition rate laser the speed was above 600 rev/min to ensure that each laser pulse hit a new spot on the target surface. For the 76 MHz repetition rate laser the maximum rotation speed of 1500 rev/min corresponded to about 300 laser pulses during the time when the target surface moved a distance of one focal spot diameter (15 μm). The laser beam was tracked parallel to the cylinder axis in order to avoid focusing into the craters formed by previous pulses.

To degas the graphite target and reduce possible surface contamination, the graphite cylinder was irradiated by the LEE laser in continuous-wave (CW) mode (with the acousto-optical Q-switch off) for a few minutes before each deposition. The cw-laser intensity of $\sim 5\times 10^5$ W/cm^2 was enough to heat the target up to 1200–1300 °C but too low to cause sublimation.

The silicon substrates were placed between 14 and 17 cm from the target surface and all depositions were performed with the substrates at room temperature. The deposi-

tion rate and the deposited film thickness were monitored by a quartz crystal microbalance sensor calibrated against data from the atomic force microscope.

C. Laser plume diagnostic

The laser plume and target were imaged with a quartz lens onto the slit of a grating spectrometer with a focusing 450 l/mm grating. Optical emission was recorded in the spectral range 200–800 nm with a linear charge coupled device (CCD) (LAMDA LS-200 optical analyzer) connected to a computer for data acquisition and analysis. The spectral resolution of the system was 1 nm. The spatial resolution of the image of ~1 mm was sufficient to separate the emission from the heated target and the expanding laser plume. The recorded spectra were corrected for variations in the grating spectral reflectivity and the spectral response of the CCD detector in order to allow temperature measurement through a Plank's radiation fit to the experimental data.

The target surface temperature was independently measured with spatial and separately with temporal resolution by two-channel optical pyrometers using interference filters to define 650 and 800 nm wavelength bands. To obtain spatial resolution, the target surface heated by the laser beam was imaged through the two filters onto a cooled CCD camera to provide space resolved temperature measurements with resolution of ~20 μm. Laser plume images were recorded with the cooled CCD video camera, the frame acquisition time was 0.03 s. When the CCD camera was replaced with two high-speed photo detectors connected to a two-channel digital oscilloscope, the temporal behavior of the surface temperature could be recorded with time resolution of 2 ns.

D. Methods for analyzing the deposited carbon films

The optical properties of the films were characterized by spectroscopic ellipsometry in the spectral range 400–800 nm. A ''VASE'' ellipsometer (J. A. Woollan Co.) was used for measurements of the real (n) and imaginary (k) parts of the complex refractive index of the deposited carbon films after prior measurement of the films thickness with atomic force microscopy (AFM).

The characteristics of the carbon bonds in the films were analyzed using Raman spectroscopy. The Raman measurements of the film evaporated on Si substrate used a Renishaw Raman Imaging microscope[3] operating in the wave number range 800–2000 cm^{-1} and using a 30 mW HeNe laser (632.8 nm) for spectra excitation. A x50 microscope objective was used to focus the laser radiation into a spot of less than 2 μm in diameter and an OD1 neutral density filter was required to prevent the carbon film from burning. The integration time of 100 s was sufficient to record spectra with adequate signal-to-noise ratio.

The particulate density in the film and the depth of craters formed during evaporation of the target were examined with optical and with high resolution scanning electron microscopy (SEM) using a field emission scanning electron microscope (Hitachi, model S4500). The surface morphology of the deposited carbon film was investigated using AFM with a NanoScope scanning probe microscope from Digital Instruments.

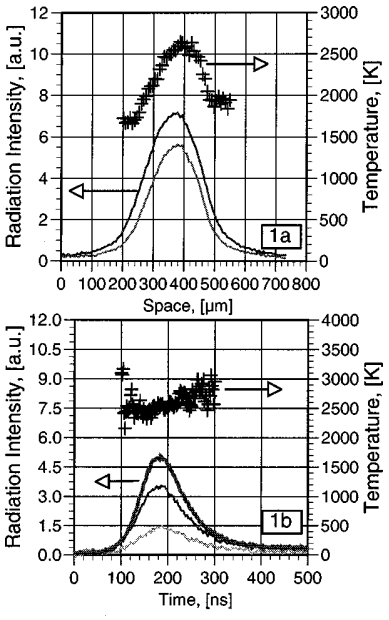

FIG. 1. Target surface temperature (crosses) for 10 kHz 120 ns laser evaporation: (a) space-resolved temperature and target radiation intensity in channels with 650 and 700 nm filters; (b) temporal behavior of the target surface temperature. Thick line is the laser pulse profile; thin lines are intensity in 650 and 800 nm channels.

III. EXPERIMENTAL RESULTS AND DISCUSSION

A. Target evaporation and vapor properties

1. Temperature measurements

A typical time-integrated, space-resolved, target surface temperature profile using 10 kHz 120 ns laser pulses scanned over the target surface is shown on Fig. 1(a). The target surface temperature was 2600 K±50 K in the area of the focal spot of ~100 μm. The target temperature in the experiments with 76 MHz 60 ps laser is in the same range but over a smaller area of about 20 μm (which is the resolution limit for space resolved temperature measurements; see Sec. II C) due to the smaller focal spot. The measured temperature was close to the sublimation temperature for carbon for a vacuum of 10^{-6} Torr.[4]

The time dependent behavior of the temperature at the target surface in the experiments using the 10 kHz laser is shown in Fig. 1(b). The graphs show the intensity of the target radiation in the 650 and 800 nm channels, as well as the laser pulse intensity profile. The measured target temperature was 2500 K±100 K, which was in good agreement with space resolved data. Unfortunately, the low signal level and poor signal to noise ratio did not allow measurement of the temperature beyond 200 ns or measurement of the cooling rate of the target between the pulses.

The emission spectrum from both the target surface and the laser plume is shown in Fig. 2. The spectrum consists on two easily distinguished parts: one is continuous radiation in the 600–800 nm range from the evaporating target surface,

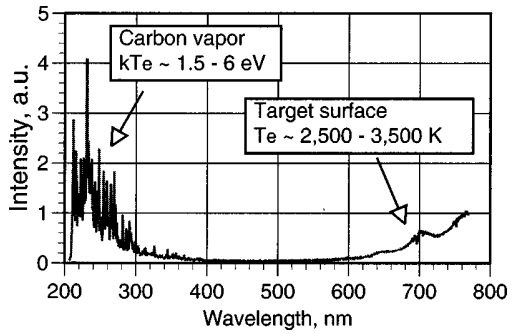

FIG. 2. Typical spectrum of laser evaporated carbon vapor and graphite target surface.

and another is line radiation below 400 nm from carbon vapor in the laser plume. The 400–600 nm spectral range is featureless. The continuum emission results from Bremsstrahlung (free-free) and recombination (free-bound) electronic recombination. The slow variation of the emission intensity with the wavelength on the long wavelength part of the spectra is possibly due to the radiation from molecular bands from the dense vapor near the target surface. The spectrum of continuous radiation is a good fit to Plank's radiation law for a temperature in the range of 2500–3500 K.

The most intense spectral lines located at 251, 258, 275, 284, 299, and 388–392 nm were identified as CII emission (ionization potential 11.26 eV), and those located at 216, 230, and 270–272 nm were identified as CIII emission (ionization potential 24.38 eV). The spectral lines intensities are not given as they varied during the evaporation. Nevertheless, the general behavior is as follows. There is rather weak radiation from neutral carbon (CI) at 248 nm; but almost equally strong line intensity from the singly ionized (CII) and doubly ionized (CIII) carbon ions. There were no CIV spectral lines detected in the spectra. On the basis of these observations we can roughly estimate the temperature in the radiating carbon plasma as $1.5\,\mathrm{eV} \leqslant T \leqslant 6\,\mathrm{eV}$.[5] Thus, the thermal velocities of the carbon ions in the laser plume expanding into vacuum should have a Maxwellian distribution with a maximum at $v_s \sim (0.5-1)\times 10^6$ cm/s.

2. Laser absorption mechanism

The experiments indicated that the average temperature was different in two zones: the solid target surface and the vapor. In conditions where the heat of vaporization of the heated volume far exceeds its thermal energy at the evaporation temperature, and for irradiances less than or equal to the value for optimal evaporation, as defined in part I of this article, then the surface temperature should equal the evaporation temperature. This was confirmed by the experimental data.

Our experimental data also indicated that the plume contained both singly and doubly ionized carbon atoms which implies that the vapor temperature is much higher than the surface temperature. This can occur in a regime where the laser intensity is absorbed not at the solid interface but at the critical density (corresponding to an electron density of 10^{21} cm^{-3} for 1.064 μm laser) in a plasma plume. The maximum temperature near the critical density can be estimated as follows:[6]

$$T_{\max}[K] = 3.594\times 10^4 (\lambda[\mu\mathrm{m}])^{4/3} \times \left(\frac{I_a}{10^9[\mathrm{W/cm^2}]}\right)^{2/3} Z^{2/3} M^{1/3}, \tag{2}$$

here Z,M are the average ion charge and mass, respectively; and λ is the laser wavelength. Taking $Z=1$, $M=12$, for the carbon vapors; $\lambda = 1.064\,\mu$m; and the intensities as given above, one obtains $T_{\max} = 5.4\times 10^4$ K (4.7 eV) for the experiments with the 10 kHz laser, and $T_{\max} = 1.4\times 10^5$ K (12 eV) for the experiments with the 76 MHz laser. The average temperature at the critical density in accordance with the predictions of the theory[2] are $T_{\mathrm{av}} = 4.5\times 10^3$ K (0.5 eV) for 10 kHz laser evaporation; and $T_{\mathrm{av}} = 2.4\times 10^4$ K (2.1 eV) for the 76 MHz case.

These last values are in reasonable agreement with the conditions in the plume estimated from the ion populations where values of 1.5–6 eV were obtained for both lasers. The experiments, therefore, indicate that the laser–target interaction falls into the well known regime for laser-produced plasmas where the absorption occurs in a plasma near the critical density surface, and the main absorption mechanism is inverse Bremsstrahlung. It is well known from numerous studies that the main mechanisms for ionization of such ablated vapors are photoionization (with multiphoton ionization as a seed process); and ionization by electron impact (which is primarily responsible for avalanche ionization and breakdown). Photorecombination and recombination by three body collisions in dense plasma are responsible for the line emission as well as the electronic transitions in the exited carbon atoms in the expanding laser plume.

3. Evaporation rate measurements

If the laser focal spot is kept on the same position on the target for several consecutive pulses a crater is produced in the target which increases by a depth d per pulse. At very high repetition rates, this leads to a growth in the density of the vapors in the crater. As a result, the laser light is likely to be absorbed in the vapor further from the solid target surface, and consequently the interaction regime changes to one less favorable in terms of evaporation efficiency. When the crater depth becomes comparable with the diameter of the focal spot, the expansion of vapors is completely different from that for a flat target. In a deep crater the thermal losses into the walls dominate the laser–target interaction process.

The importance of laser scanning over the target surface was demonstrated by measuring the evaporation rate from the target irradiated by a predetermined number of 120 ns duration laser pulses at 10 kHz repetition rate at the optimum laser intensity of 6×10^8 W/cm^2. The Q-switched laser was gated to achieve the desired number of laser pulses N_p. The evaporation rate was deduced from the volume V_{evap} of the evaporated cone-like crater on the target surface, measured with both an optical microscope and the SEM for a given number of pulses:

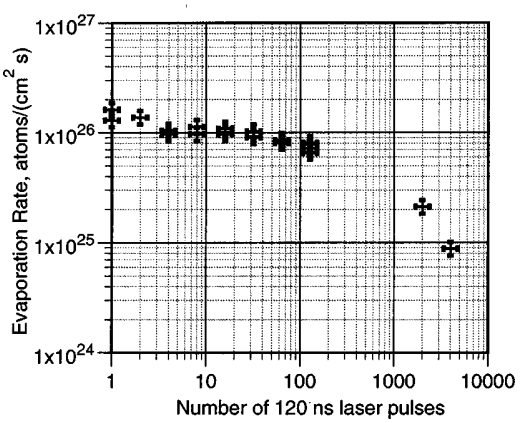

FIG. 3. Evaporation rate vs the number of 120 ns laser pulses at a 10 kHz repetition rate.

$$R_{\text{evap}}=\frac{V_{\text{evap}}\rho N_A}{M_C S_{\text{foc}} t_p N_p}\,[\text{atoms}/(\text{cm}^2\,\text{s})]; \tag{3}$$

here $\rho=2.26\ \text{g/cm}^3$ is the graphite target density, $N_A=6.02\times10^{23}$ is the Avogadro number, $M_C=12$ for carbon, and S_{foc} is the focal spot area.

The variation of average evaporation rate versus the number of laser pulses is shown in Fig. 3. For a single 120 ns pulse the measured rate $R_{\text{evap}}=(1.4\pm0.2)\times10^{26}$ atoms/cm^2 s is relatively close to the theoretical estimate for the maximum number of evaporated atoms of 10^{27} atoms/cm^2 s.[2] The measured rate corresponds to a crater depth of $(1.5\pm0.2)\ \mu$m per pulse. After about ten successive pulses fired into the same spot on the target, the average evaporation rate dropped about twofold; while after 2000 shots (0.5 s at 10 kHz repetition rate) it was an order of magnitude below the single-pulse rate. We note that, in general, the evaporation rate behaves in a similar manner to that reported in Ref. 7 from experiments using a 10 Hz, 17 ns, XeCl excimer laser, where the ablation depth in a graphite target was observed to decrease after 100 laser pulses.

Based on these data, we performed subsequent evaporation experiments with the 10 kHz laser using a rotating target, therefore, scanning over the target surface with the scanning speed adjusted so that each laser shot hit a fresh part of the target surface (see Sec. II B above). The maximum scanning speed of about 400 cm/s meant that when using the 76 MHz laser, almost 300 laser pulses hit the same spot on the target. Nevertheless, because the Antares pulses were very low energy, this scanning speed was still five times higher than the minimum needed to obtain evaporation without the creation of a crater (see Sec. III C, Ref. 2).

B. Properties of the deposited carbon films

1. Laser plume images, particulates emission from the target

The most general reasons for poor quality in a thin film prepared by PLD are inhomogeneities in the target material and spatial and temporal variations of the laser intensity on the target surface. When high energy laser pulses are used for ablation, such inhomogeneities can lead to the plume being contaminated by the ejection solid particulates or liquid droplets which then contaminate the films. However, if the number of atoms evaporated per single pulse were reduced, via a reduction in the single pulse laser energy, to the point where fewer atoms were evaporated than needed to create a single particulate or droplet, no such defects would be expected to appear on the substrate.

It is straightforward to estimate the number of evaporated particles per laser pulse and this is shown in Table I for three different lasers at various repetition rates. To provide a meaningful comparison we shall consider the optimal regime for evaporation of carbon in each case [see Eq. (7) in Ref. 2]. The temperature along with the evaporation rate is proportional to the product $I_a\cdot(t_p)^{1/2}$ and remains constant in the optimal evaporation regime. Therefore, the number of the evaporated atoms per single pulse $N_{\text{per pulse}}\sim S_{\text{foc}}t_p$.[2]

As is evident, the maximum number of evaporated carbon atoms per single 60 ps laser pulse is approximately five orders of magnitude less than that for a conventional 10 ns pulse laser. This means that the formation of micron size particulates is virtually impossible with picosecond lasers, because a 1 μm size cluster consists of about 10^{11} carbon atoms. Put bluntly, the number of atoms evaporated per pulse is too small to form a macroscopic cluster.

This conclusion is validated by the images of different laser plumes shown in Figs. 4(a) and 4(b). The left image [Fig. 4(a)] is the laser plume using 10 kHz repetition rate laser averaged over ~300 pulses (~33 ms). Tracks of hot particles are still quite evident in the plume even after this averaging (although the number of hot particle tracks is still much smaller then generally observed using a high energy low repetition rate laser). The right hand image, Fig. 4(b),

TABLE I. Optimized ablation performance for convention, high repetition rate, and ultrahigh repetition rate PLD.

Ablation type	Laser repetition rate (Hz)	Laser pulse duration (ns)	Laser pulse energy (mJ)	Optimal laser intensity (W/cm^2)	Focused beam area (cm^2)	Number of atoms per pulse
Conventional	30	10	1000	1.6×10^9	0.063	1.7×10^{18}
High repetition rate	10^4	120	3	5×10^8	5×10^{-5}	5×10^{15}
Ultrahigh repetition rate	76×10^6	0.06	0.0018	2×10^{10}	10^{-6}	3×10^{12}

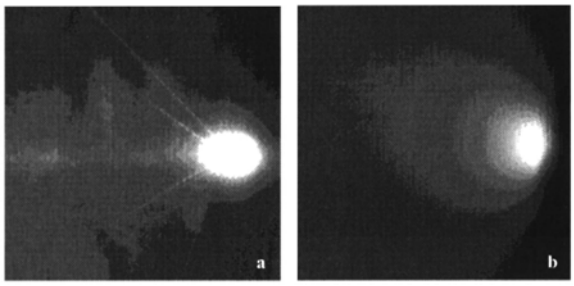

FIG. 4. Laser plume images in experiments with the 10 kHz (a) and 76 MHz (b) lasers.

was obtained for a 76 MHz repetition rate evaporation. The plume is smooth, there is no discernible disturbance in the continuous glow of carbon vapor. The exposure time for the image was also 33 ms.

2. Studies of film homogeneity with optical microscopy and scanning electron microscopy

Optical microscope images of thin carbon films deposited on polished Si wafers using either the 10 kHz, 120 ns laser, and the 60 ps, 76 MHz laser are shown in Figs. 5(b) and 5(c). For comparison we also present in Fig. 5(a) the image of a carbon film evaporated using the conventional PLD with a 10 ns, 30 Hz, 100 mJ Nd:YAG laser. All the substrates were positioned 20 mm from the target and the evaporation time was 10 min in each case.

The images reveal strikingly different results for the particle density on the substrate. The film deposited with the 30 Hz laser was covered with both spherical and irregular particles in the micron size range with the particle density above 1000 mm^{-2}. This is quite typical of conventional evaporation with powerful lasers.[8] The ejection of such hot particles during the evaporation process was clearly seen as a glowing shower of ''sparks'' from the focal spot. In contrast, the density of micron sized particles on the substrate was less than 100 per mm^2 when the film was deposited with the 10 kHz evaporation. Most significantly, however, it was difficult to find *any* particles on the surface of the film deposited with the 76 MHz, 60 ps laser. What particles did exists, at a density $<1/mm^2$, seemed to be dust which did not originate from the vapors.

High resolution SEM images of the films evaporated using the 10 kHz and 76 MHz lasers [Figs. 6(a)–6(f)] show smooth and continuous film surfaces with at worst 20–100 nm size irregularities. A distinguishing feature of the films

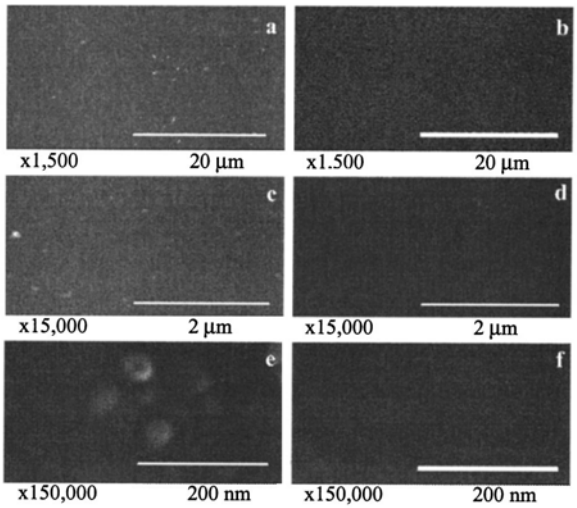

FIG. 6. SEM images with magnification 1,5 K (a), (b), 15 K (c), (d), and 150 K (e), (f) of carbon films evaporated with the 10 kHz laser (a), (c), (e) and the 76 MHz laser (b), (d), (f).

evaporated at 10 kHz is a larger number of particles with a much higher electron emission than the surrounding film. The images are similar in appearance to those of diamond-like carbon films produced by direct current glow discharge chemical vapor deposition (dc-CVD) process.[9] The efficiency of secondary electron emission is known to be much higher for nanosized diamond that for other graphite material.[10] Therefore, we speculate that these nanosize clusters consist of diamond-bonded carbon.

3. Film morphology

The surface morphology of carbon films between 25 and 120-nm-thick evaporated with the 10 kHz and with the 76 MHz lasers was investigated with atomic force microscopy in the tapping mode for improved resolution [Figs. 7(a) and 7(b)]. According to standard procedure, the background plane was deconvolved from the raw data prior to the surface roughness measurements. AFM images of the 10 kHz evaporated films revealed gently sloping ''hills'' on the surface with an atomically smooth flat ''valleys'' in between. The width of the hills lay in the range of 20–100 nm, similar to those seen in the SEM images, while their height was 2–20 nm, and seemed to be independent of the film thickness, at least for the films studied. The measured root-mean-square

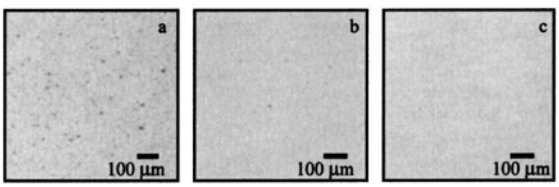

FIG. 5. Optical microscope images of deposited carbon film with a 10 ns 30 Hz laser (a), with a 120 ns 10 kHz laser (b), and with a 60 ps 76 MHz laser (c).

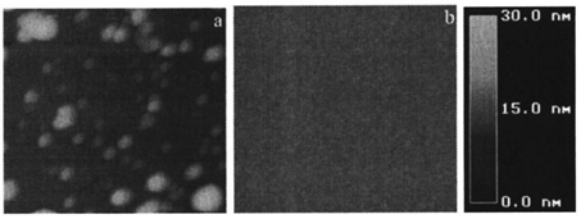

FIG. 7. AFM surface profile of 1×1 μm^2 area of carbon film deposited mica with the 10 kHz laser (a) and the 76 MHz laser (b).

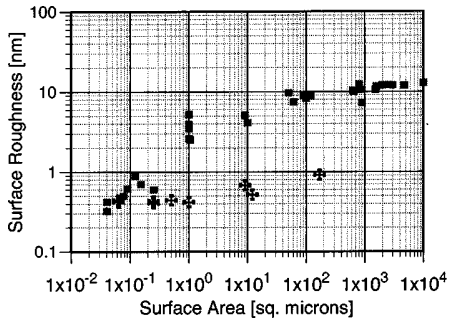

FIG. 8. The rms surface roughness vs the analyzed surface area of the film; squares are for 10 kHz evaporation, and crosses are for 76 MHz evaporation.

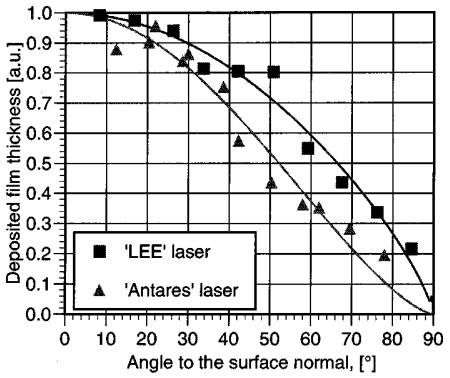

FIG. 9. Deposited carbon film thickness vs angle to the laser beam axis for the 10 kHz laser deposition (squares) and for the 76 MHz laser (triangles) deposition. Best curve fittings are $f(\theta)\sim\cos^{0.75}(\theta)$ for 10 kHz and $f(\theta)\sim\cos^{1.4}(\theta)$ for 76 MHz laser deposition.

(rms) surface microroughness depended on the film area analyzed and had a saturation-like behavior at the level of ~12 nm [Fig. 7(c)].

The 76 MHz evaporated films were almost free of submicron irregularities and appeared to be atomically smooth with surface variations within ±1 nm [Fig. 7(b)]. The rms roughness was <1 nm over the whole measured area up to $13\times13\ \mu m^2$ [Fig. 7(c)]. The occasional particle on the surface did not influence the roughness analysis. These data show that evaporation with low energy ultrahigh repetition rate lasers provides a way for laser deposition of particulate-free films with surface smoothness at the atomic level.

4. Angular distribution of the ablated carbon vapor, deposition rate, and homogeneity of the film thickness

The angular distribution of the ablated carbon vapor was measured from variations in the thickness of the deposited carbon film. The thickness measurements were performed by means of optical ellipsometry. The film thickness was monitored during the evaporation process by a quartz crystal sensor positioned at a fixed angle of $\theta=22.5°$ relative to the target normal (and to the axis of the laser beam). The silicon wafers were placed around a semicircle in the vacuum chamber at the distance of 170 mm from the focal spot on the target.

The results for both 10 kHz and 76 MHz lasers were presented on Fig. 8. The fits to the experimental data suggest the source distribution $f(\theta)\sim\cos^{0.75}(\theta)$ for 10 kHz, and $f(\theta)\sim\cos^{1.42}(\theta)$ for the 76 MHz lasers. Such angular distributions are relatively close to an ideal hemispherical distribution with an inverse square relationship between the distance to the substrate and the deposited film thickness. The distributions follow from the fact that the focal spot is very small relative to the target-substrate distance, and also demonstrate that collision-less expansion of the ablated vapor occurs in the plume.

The deposition rate on a substrate located $R_0=150$ mm from the target was in the range of 2–6 Å/s for the 10 kHz laser, and 0.8–2.5 Å/s for the 76 MHz laser. To compare these rates with those from conventional PLD, we assumed for simplicity, that the deposition rate depended via an inverse square law on the target-substrate separation, R_0. Literature values for conventional PLD were extracted from Ref. 7 for $R_0=3$ cm at 2 Å/s, while a higher rate of 3.5–5.5 Å/s was measured in Ref. 11 for $R_0=3.5$ cm. These deposition rates are ~25 times lower than those in the experiments presented here for the 10 kHz laser, and 3–10 times lower than that achieved with the 76 MHz laser (which did not achieve the optimal evaporation intensity).

To illustrate the excellent thickness homogeneity of the ultrafast laser deposition process, diamond-like carbon film was deposited simultaneously on two 4 in. silicon wafers placed next to each other 170 mm from the target. The thickness of the deposited film measured by optical ellipsometry was within ±5% over an area of ~250 cm^2.

5. Refractive index and band gap measurements

Figure 9 show the index of refraction (n) and extinction coefficient (k) obtained by ellipsometry of the carbon film deposited on a Si wafer with 10 kHz and 76 MHz lasers. For comparison, the refractive indices for graphite and natural diamond are also presented.[12] The refractive index variation with wavelength is closest to that of graphite although the exact values are slightly higher than those for graphite.

Combining the measured refractive index and extinction coefficients with the corresponding photon energies $h\nu$, the band gap energy E_g were estimated by using the Tauc relation:[13–15] $\epsilon(h\nu)=A(h\nu-E_g)^2/(h\nu)^2$, where $\epsilon=2nk$ and A is a constant. The tangential extrapolation of the Tauc plot $(h\nu\epsilon^{1/2})$ vs $h\nu$ provides the optical band gap E_g of the film at the intersection with the $h\nu$ axis (Fig. 10). The optical band gap was 0.5 eV for the 76 MHz laser and 0.7 eV for 10 kHz laser. The reported optical band gap for amorphous carbon films deposited by means of laser ablation is usually 0.4–2.3 eV, depending on the substrate temperature[11] and laser intensity.[15]

6. Raman spectra measurements

The Raman spectra for films produced by either the 10 kHz or 76 MHz lasers were very similar: they show a broad band with a maximum near 1500 cm^{-1}. This indicates that a significant fraction of the amorphous carbon film is a mixture of sp^2 and sp^3 bonded carbon.[16] A typical Raman visible (632.8 nm) spectrum of the deposited carbon film is shown

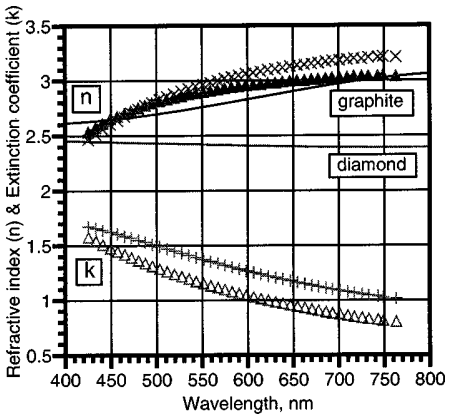

FIG. 10. Refractive indices (n) and extinction coefficients (k) for carbon films evaporated with the 10 kHz laser (crosses) and the 76 MHz lasers (triangles).

in Fig. 11. The spectrum was fitted with three Gaussians and is dominated by the ''G'' peak whose maximum lies approximately at 1500 cm^{-1}, but also shows a shoulder due to the ''D'' peak located at around 1300 cm^{-1}. The Raman spectra are similar to those obtained for evaporated amorphous carbon films, and both D and G peaks attributed to graphitic sp^2 bonding (Fig. 12).[17,18] To achieve a reasonable fit to the experimental results it was always necessary to add the third peak at 1160 cm^{-1}, which is referred in some article as due to the regions of microcrystalline diamond or amorphous diamond within an amorphous carbon matrix.[16,19] These microcrystalline diamonds could be responsible for higher secondary electron emission in SEM images (see Sec. III B 1).

IV. CONCLUSION

Ultrafast laser ablation has been studied in order to demonstrate that a new opportunity exists for PLD technology. The experiments on ultrafast PLD were carried out with a graphite target, which is one of the most refractory material in nature. The main advantage of employing high repetition rate in conjunction with low energy, picosecond laser pulses for PLD have been demonstrated via almost complete elimination of particles on the film. This has, up until now, been the major drawback of PLD technique. It was also shown

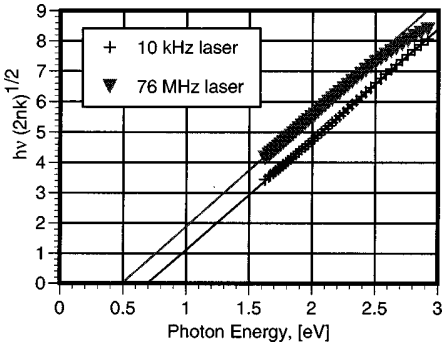

FIG. 11. Tauc plot for determining the optical band gaps of the films presented on Fig. 10.

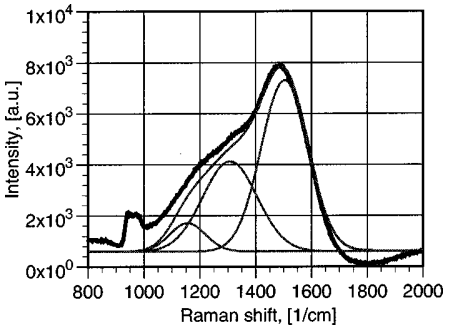

FIG. 12. Raman spectrum of amorphous carbon film containing sp^2 and sp^3 components, and synthesized data resulting from contributing peak analysis.

that very high deposition rates could be achieved in experiments with high repetition rate laser ablation. A deposition rate of ~5 Å/s was achieved at a target-substrate distance of 150 mm, which is 10–25 times higher than that reported with conventional high energy low repetition rate nanosecond lasers. The high deposition rate combined with an excellent film thickness uniformity (±5% thickness variation over ~250 cm^2), and exceptional film surface quality are unique features of this process. The rms microroughness of the deposited films saturated at 12 nm in the experiments with the 10 kHz laser, and demonstrated almost atomic smoothness of the films ablated by 76 MHz laser with rms microroughness below 1 nm.

Temperature measurements of the laser plume in the range of 1.5–6 eV suggest that laser absorption occurs in the plasma vapors near the critical density, and the main absorption mechanism is inverse Bremsstrahlung. The importance of laser scanning over the target surface was demonstrated by measuring the reduction in the evaporation rate as a larger number of laser pulses were fired at the same target spot.

Although the achievement of diamond-like properties of the ablated carbon foils was not the main purpose of this work, the SEM images, optical band gap measurements, and Raman spectra measurements prove the potential for effective deposition of amorphous diamond-like carbon (DLC) films using high repetition rate laser ablation.

The method can be extended for the formation of structured and multilayered films of different materials, and for production of other carbonaceous structures such as carbon nanotubes, fullerenes and diamond-like carbon material. The results of these experiments will be presented elsewhere.

ACKNOWLEDGMENTS

We would like to convey our appreciation to T. Senden for his assistance with the AFM measurements, to S. Hatch for her assistance with the ellipsometry measurements, and to A. Hoffman for useful discussions and presenting results on DLC films produced by dc-CVD process prior to publication. One of the authors (A.V.R.) gratefully acknowledges the receipt of a Queen Elizabeth II Fellowship.

[1] *Pulsed Laser Deposition of Thin Films*, edited by D. B. Chrisey and G. K. Hubler (Wiley, New York, 1994).
[2] E. G. Gamaly and A. V. Rode, J. Appl. Phys. **85**, 4213 (1999).

[3] I. P. Hayward, K. J. Baldwin, D. M. Hunter, D. N. Batchelder, and G. D. Pitt, Diamond Relat. Mater. **4**, 617 (1995).
[4] O. Pierson, *Handbook of Carbon, Graphite, Diamond, and Fullerenes* (Noyes, Park Ridge, 1993).
[5] W. Lochte-Holtgreven, in *Plasma Diagnostics*, edited by W. Lochte-Holtgreven (North–Holland, Amsterdam, 1968), pp. 135–213; I. I. Sobelman, L. A. Vainshtein, and E. A. Yukov, *Excitation of Atoms and Broadening of Spectral Lines* (Springer, Berlin, 1981).
[6] Yu. V. Afanasiev, E. G. Gamaly, O. N. Krokhin, and V. B. Rozanov, Sov. Phys. JETP **44**, 311 (1976).
[7] W. Kautek, S. Pentzien, A. Conradi, J. Krüger, and K.-W. Brzezinka, Appl. Surf. Sci. **106**, 158 (1996).
[8] L.-C. Chen, in *Pulsed Laser Deposition of Thin Films*, edited by D. B. Chrisey and G. K. Hubler (Wiley, New York, 1994), pp. 167–198.
[9] I. Gouzman, A. Hoffman, G. Gomtet, L. Hellner, G. Dujardin, and M. Petravic, Appl. Phys. Lett. (accepted).
[10] A. Hoffman, S. Prawer, and R. Kalish, Diamond Relat. Mater. **1**, 440 (1992).
[11] J. Bulir, M. Jelinek, V. Vorlicek, D. Chvostova, and L. Soukur, J. Non-Cryst. Solids **188**, 118 (1995).
[12] D. F. Edwards and H. R. Phillipp, in *Handbook of Optical Constants of Solids I*, edited by E. D. Palik (Academic, San Diego, 1985); A. Borghesi and G. Guizzetti, in *Handbook of Optical Constants of Solids II*, edited by E. D. Palik (Academic, San Diego, 1991).
[13] J. Tauc, R. Grigorovici, and A. Vancu, Phys. Status Solidi **15**, 627 (1966).
[14] N. Savvides, J. Appl. Phys. **59**, 4133 (1986).
[15] H. C. Ong and R. P. Chang, Phys. Rev. B **55**, 13213 (1997).
[16] P. R. Chalker, in *Diamond and Diamond-Like Films and Coatings*, edited by R. E. Clausing, L. L. Horton, J. C. Angus, and P. Koidl (Plenum, New York, 1991), p. 127; P. K. Bachmann and D. U. Wiechert, *ibid.*, p. 677.
[17] M. P. Siegal, L. J. Martinez-Miranda, N. J. DiNardo, D. R. Tallant, J. C. Barbour, and P. N. Provencio, Invited paper presented at SPIE High-Power Laser Ablation Symposium, SPIE paper #3343-91, Santa Fe, New Mexico, April 1998.
[18] K. W. R. Gilkes, H. S. Sands, D. N. Batchelder, J. Robertson, and W. I. Milne, Appl. Phys. Lett. **70**, 1980 (1997).
[19] J. Schwan, S. Ulrich, H. Roth, H. Ehrhardt, S. R. P. Silva, J. Robertson, R. Samlenski, and R. Brenn, J. Appl. Phys. **79**, 1416 (1996).